Majorana corner states in a two-dimensional magnetic topological insulator on a high-temperature superconductor

Tao Liu,[1] James Jun He,[2] and Franco Nori (野理)[1,3,*]

[1]*Theoretical Quantum Physics Laboratory, RIKEN Cluster for Pioneering Research, Wako-shi, Saitama 351-0198, Japan*
[2]*RIKEN Center for Emergent Matter Science, Wako, Saitama 351-0198, Japan*
[3]*Department of Physics, University of Michigan, Ann Arbor, Michigan 48109-1040, USA*

(Received 19 June 2018; revised manuscript received 1 November 2018; published 13 December 2018)

Conventional n-dimensional topological superconductors (TSCs) have protected gapless $(n-1)$-dimensional boundary states. In contrast to this, second-order TSCs are characterized by topologically protected gapless $(n-2)$-dimensional states with the usual gapped $(n-1)$ boundaries. Here, we study a second-order TSC with a two-dimensional (2D) magnetic topological insulator proximity coupled to a high-temperature superconductor, where Majorana bound states (MBSs) are localized at the corners of a square sample with gapped edge modes. Due to the mirror symmetry of the hybrid system considered here, there are two MBSs at each corner for both cases: d-wave and $s_{\pm}$-wave superconducting pairing. We present the corresponding topological phase diagrams related to the role of the magnetic exchange interaction and the pairing amplitude. A detailed analysis, based on edge theory, reveals the origin of the existence of MBSs at the corners of the 2D sample, which results from the sign change of the Dirac mass emerging at the intersection of any two adjacent edges due to pairing symmetry. Possible experimental realizations are discussed. Our proposal offers a promising platform for realizing MBSs and performing possible non-Abelian braiding in 2D systems.

DOI: 10.1103/PhysRevB.98.245413

I. INTRODUCTION

The study of nontrivial topological bands has led to the advent of a plethora of novel phases of matter characterized by topological invariants, which are independent of their microscopic details. These phases are characterized by a finite energy gap in the bulk and protected gapless states at their edges, with unusual properties. Recent years have seen a great deal of theoretical and experimental efforts towards the realization and exploration of Majorana zero modes (MZMs) in topological phases of quantum matter [1–6]. MZMs are zero-energy bound quasiparticles emerging at the boundaries of topological superconductors (TSCs), which are expected to exhibit exotic non-Abelian anyon statistics. This distinct feature makes MZMs promising for studying fault-tolerant topological quantum computations [7–9]. Several promising condensed-matter systems potentially hosting MZMs have been proposed, including spin-orbit coupling semiconductor nanowire/superconductor hybrid structures [10–15], ferromagnetic atomic chains on superconductors [16–19], topological insulator/superconductor hybrid structures [20–24], and hybrid systems with unconventional superconductivity [25–29], among others.

The nontrivial topological band structure of superconductor systems is the essential ingredient for the creation of MZMs in previous proposals, which is characterized by the bulk-boundary correspondence. Very recently, the concept of higher-order topological insulators (TIs) [30–41] was put forward, where the usual form of the bulk-boundary correspondence is no longer applicable. As a new type of topological phase, it has no gapless surface states on three-dimensional (3D) insulators and gapless edge states on two-dimensional (2D) ones. Nevertheless, the n-dimensional systems have protected gapless $(n-2)$-dimensional states with the usual gapped $(n-1)$-dimensional boundaries. For example, a second-order TI in three dimensions hosts one-dimensional gapless modes in its hinges, while a second-order 2D TI has zero-energy states localized at its corners.

In terms of second-order TSCs in two dimensions, the MZMs will emerge at its corner, i.e., Majorana corner states (MCSs), which are localized at the intersection of two gapped topologically distinct edges. The study of MCSs is still at a very exploratory stage, and a few works were recently reported: high-temperature Majorana Kramers pairs with time-reversal symmetry localized at corners [42–44], MCSs in a p-wave superconductor with an in-plane external magnetic field [45], Majorana bound states (MBSs) in a second-order Kitaev spin liquid [46], and 2D and 3D second-order TSCs with $(p+ip)$ and $(p+id)$ superconductors [47].

In this paper, we study a kind of hybrid superconducting structure with a 2D magnetic TI and a high-temperature superconductor. This 2D magnetic TI shows a quantum anomalous Hall effect and has been intensively investigated [48–50]. These can now be experimentally realized by introducing magnetic doping with Cr, V, or Mn ions [51–57] or inducing proximity-induced ferromagnetism with a ferromagnetic insulator (FI) (i.e., TI/FI heterostructure) [57,58] to TI. Moreover, chiral MZMs are currently experimentally observed in a magnetic TI through the proximity effect to a conventional s-wave superconductor [24]. Additionally, the cuprate-based [59–61] and iron-based [62–66] high-temperature superconductors have been experimentally reported to induce topological superconductivity. One important open question is whether

*fnori@riken.jp

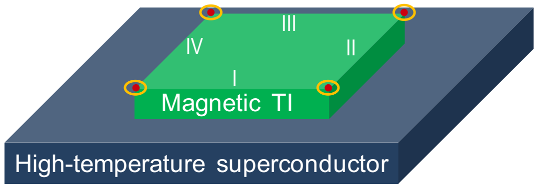

FIG. 1. Schematic view showing a magnetic TI approximated by a high-temperature superconductor. The Majorana bound states are located at the four corners of the green square sample. I, II, III, and IV label the four edges of the lattice.

a 2D magnetic TI approximated by a high-temperature superconductor can exhibit a second-order TSC hosting MBSs localized at their corners and how the magnetic exchange interaction in the 2D magnetic TI influences the second-order topological features. Here, we show that a second-order TSC can be achieved by a 2D magnetic TI grown on a cuprate-based or iron-based high-temperature superconductor. Although the hybrid superconductor system is in the topologically trivial regime with an insulating gap, there are MBSs localized at each corner of a square sample. The existence of MCSs requires a magnetic insulator in a topologically nontrivial regime with protected chiral edges. These edge states can be gapped out once the high-temperature superconductor pairing (e.g., d-wave pairing) is introduced. Due to the superconducting pairing symmetry, the gapped two adjacent edges intersecting at corners have opposite Dirac masses, where MCSs are generated at one corner. Because the hybrid system considered here has mirror symmetry, there are two MBSs at each corner. In this paper, in order to demonstrate this second-order TSC, we apply an intuitive edge argument. Moreover, we derive the topological phase diagrams involving the role of magnetic exchange interaction and pairing amplitude. The proposed second-order TSC provides an alternate method for realizing MBSs. This suggests a promising platform for braiding MZMs in 2D systems, which may not be achieved for chiral Majorana modes in conventional 2D TSCs [67].

This paper is organized as follows: in Sec. II, we consider a minimal model on a square lattice describing a magnetic TI approximated by a high-temperature superconductor. Section III presents the results of magnetic TIs grown on either a d-wave or an $s_{\pm}$-wave superconductor. An intuitive edge argument is given, and topological phase diagrams of hybrid high-temperature superconducting systems are provided. Section IV describes the experimental feasibility of hybrid superconducting systems and concludes this paper.

II. MODEL

We here consider a minimal model on a square lattice, which describes a magnetic TI approximating a high-temperature superconductor, as shown in Fig. 1. The tight-binding Hamiltonian is given by $H = H_{\rm t} + H_{\rm so} + H_{\rm z} + H_{\rm sc} + \text{H.c.}$,

$$H_{\rm t} = \frac{m_0}{2}\sum_{j,s} c^{\dagger}_{j,a,s}\sigma_z^{ab}c_{j,b,s} + \frac{m_x}{2}\sum_{j,s} c^{\dagger}_{j,a,s}\sigma_z^{ab}c_{j+x,b,s} + \frac{m_y}{2}\sum_{j,s} c^{\dagger}_{j,a,s}\sigma_z^{ab}c_{j+y,b,s} - \frac{\mu}{2}\sum_{j,\sigma,s} c^{\dagger}_{j,\sigma,s}c_{j,\sigma,s}, \tag{1}$$

$$H_{\rm so} = -i\frac{\lambda_{\rm so}}{2}\sum_{j,v=x,y} c^{\dagger}_{j,a,\alpha}s_v^{\alpha\beta}\sigma_x^{ab}c_{j+v,b,\beta}, \tag{2}$$

$$H_{\rm z} = \frac{\lambda_z}{2}\sum_{j,\sigma}(c^{\dagger}_{j,\sigma,\uparrow}c_{j,\sigma,\uparrow} - c^{\dagger}_{j,\sigma,\downarrow}c_{j,\sigma,\downarrow}), \tag{3}$$

$$H_{\rm sc} = \Delta_0\sum_j c^{\dagger}_{j,\sigma,\uparrow}c^{\dagger}_{j,\sigma,\downarrow} + \frac{\Delta_x}{2}\sum_j c^{\dagger}_{j,\sigma,\uparrow}c^{\dagger}_{j+x,\sigma,\downarrow} + \frac{\Delta_y}{2}\sum_j c^{\dagger}_{j,\sigma,\uparrow}c^{\dagger}_{j+y,\sigma,\downarrow}, \tag{4}$$

where these terms are the kinetic term $H_{\rm t}$, spin-orbit coupling $H_{\rm so}$, Zeeman coupling $H_{\rm z}$, and superconducting pairing $H_{\rm sc}$. Also, s_i and σ_i are Pauli matrices denoting the electron spins $(\uparrow,\downarrow)$ and orbitals (a, b), respectively. The $c_{j,a,s}$ is the fermion operator at site j, m_0 is the orbital-dependent on-site energy, and m_x and m_y are the intraorbital hopping amplitudes along the x and y axes, while μ is the chemical potential. Moreover, $\lambda_{\rm so}$ is the spin-orbital coupling strength, and λ_z is the exchange field amplitude along the z axis induced by the magnetization. The superconducting pairing terms Δ_0, Δ_x, and Δ_y are combined to characterize $d_{x^2-y^2}$- and $s_{\pm}$-wave pairing.

According to Eqs. (1)–(4), the Bogoliubov–de Gennes (BdG) Hamiltonian can be written as $\mathcal{H}_{\rm BdG} = \sum_{\mathbf{k}}\Psi^{\dagger}_{\mathbf{k}}H_{\rm BdG}(\mathbf{k})\Psi_{\mathbf{k}}$, where $\Psi_{\mathbf{k}} = (c_{\mathbf{k},a,\uparrow}, c_{\mathbf{k},a,\downarrow}, c_{\mathbf{k},b,\uparrow}, c_{\mathbf{k},b,\downarrow}, c^{\dagger}_{-\mathbf{k},a,\downarrow}, -c^{\dagger}_{-\mathbf{k},a,\uparrow}, c^{\dagger}_{-\mathbf{k},b,\downarrow}, -c^{\dagger}_{-\mathbf{k},b,\uparrow})^T$,

$$H_{\rm BdG}(\mathbf{k}) = m(k)\sigma_z\tau_z + \lambda_{\rm so}[\sin(k_x)s_x + \sin(k_y)s_y]\sigma_x\tau_z + \lambda_z s_z - \mu\tau_z + \Delta(k)\tau_x; \tag{5}$$

here, $m(k)$ and $\Delta(k)$ are

$$m(k) = m_0 + m_x\cos(k_x) + m_y\cos(k_y), \tag{6}$$

$$\Delta(k) = \Delta_0 + \Delta_x\cos(k_x) + \Delta_y\cos(k_y), \tag{7}$$

where τ_i $(i = x, y, z)$ are Pauli matrices in the Nambu particle-hole space.

The Hamiltonian $H_{\rm BdG}(\mathbf{k})$ is invariant under a particle-hole symmetry $\Theta = \tau_y s_y\mathcal{K}$, with $\mathcal{K}$ being the complex conjugation operator, a mirror-reflection symmetry $\mathcal{M}_z = is_z\sigma_z$, a fourfold rotational symmetry $C_4 = e^{-i\frac{\pi}{4}s_z}$, and an inversion symmetry $\mathcal{P} = \sigma_z$,

$$\Theta H_{\rm BdG}(k_x,k_y)\Theta^{-1} = -H_{\rm BdG}(-k_x,-k_y), \tag{8}$$

$$\mathcal{M}_z H_{\rm BdG}(k_x,k_y)\mathcal{M}_z^{-1} = H_{\rm BdG}(k_x,k_y), \tag{9}$$

$$C_4 H_{\rm BdG}(k_x,k_y)C_4^{-1} = H_{\rm BdG}(-k_y,k_x), \tag{10}$$

$$\mathcal{P} H_{\rm BdG}(k_x,k_y)\mathcal{P}^{-1} = H_{\rm BdG}(-k_x,-k_y). \tag{11}$$

III. RESULTS

A. *d*-wave pairing

We first consider a magnetic TI grown on a d-wave cuprate high-temperature superconductor that has been widely investigated in experiments [59–61]. For a d-wave superconductor with $d_{x^2-y^2}$-wave symmetry, the pairing amplitude satisfies

$$\Delta_0 = 0, \quad \Delta_x = -\Delta_y = \Delta_1. \tag{12}$$

To explore whether the hybrid system of a magnetic TI/d-wave superconductor exhibits second-order nontrivial topological phases, which support Majorana bound states at each corner of a square sample, we first calculate the energy-band spectrum of the system. The 2D magnetic insulator is in the topologically nontrivial regime when the system parameters satisfy

$$||m_x| - |m_y|| < |m_0 \pm \lambda_z| < |m_x| + |m_y|. \tag{13}$$

Figures 2(a) and 2(b) show the energy-band structure of a 2D magnetic TI nanoribbon along the x and y directions, respectively. The red lines represent two degenerate gapless chiral edge states characterized by the Chern number $\mathcal{N} = 2$. The zero-energy edge states in the y and x directions exist at the $k_x = 0$ and $k_y = 0$ points with the parameters considered, respectively.

When a $d_{x^2-y^2}$ pairing is added to the magnetic TI, the chiral edges are gapped out [see red lines in Figs. 2(c) and 2(d)]. In this case, the hybrid system is in a topologically trivial regime with $\mathcal{N} = 0$. However, by calculating the eigenenergies of a finite square sample, two quite localized zero-energy states emerge at each corner, as shown in Fig. 2(e). Due to particle-hole symmetry Θ, these zero-energy corner states are MZMs known as Majorana corner states. The inset in Fig. 2(e) exhibits the symmetrical eigenenergies with particle and hole bands. Figure 3 shows the BdG energy spectrum with open boundary conditions in the x and y directions as a function of λ_z. The eightfold-degenerate localized zero-energy MCSs states are indicated by the red curves, which exist only in finite amplitudes of the exchange field.

Figure 4 shows the topological phase diagram of the magnetic TI/$d_{x^2-y^2}$ high-temperature superconductor hybrid system in the (m_0, λ_z) plane, which reveals three distinct phases: (i) second-order topological superconductor with MCSs, (ii) chiral MZMs characterized by a finite Chern number $\mathcal{N}$, and (iii) topologically trivial states $\mathcal{N} = 0$ with zero chiral MZMs and MCSs. The phase boundaries are determined by the zero eigenenergy of the BdG Hamiltonian in Eq. (5) at the four corners of the Brillouin zone of a square lattice, i.e., $\Gamma = (0, 0)$, $X = (0, \pi)$, $Y = (\pi, 0)$, and $M = (\pi, \pi)$, where Γ and M are two high-symmetry points. The energies at these points are

$$E_\Gamma = \pm\mu \pm (m_0 + m_x + m_y) \pm \lambda_z, \tag{14}$$

$$E_M = \pm\mu \pm (m_0 - m_x - m_y) \pm \lambda_z, \tag{15}$$

$$E_X = \pm\sqrt{(\mu \pm m_0 \pm m_x \mp m_y)^2 + 4\Delta_1^2} \pm \lambda_z, \tag{16}$$

$$E_Y = \pm\sqrt{(\mu \pm m_0 \mp m_x \pm m_y)^2 + 4\Delta_1^2} \pm \lambda_z. \tag{17}$$

In addition, the existence of MCSs requires the 2D magnetic insulator in the topologically nontrivial regime [see Eq. (13)]. All these determine the topological phase diagram shown in Fig. 4.

In order to intuitively understand the appearances of MBSs at the corners, we apply the edge theory (see, e.g., [2,42,45]). Due to the mirror-reflection symmetry $\mathcal{M}_z$, the BdG Hamiltonian can be written in the block-diagonal form by a unitary transformation U,

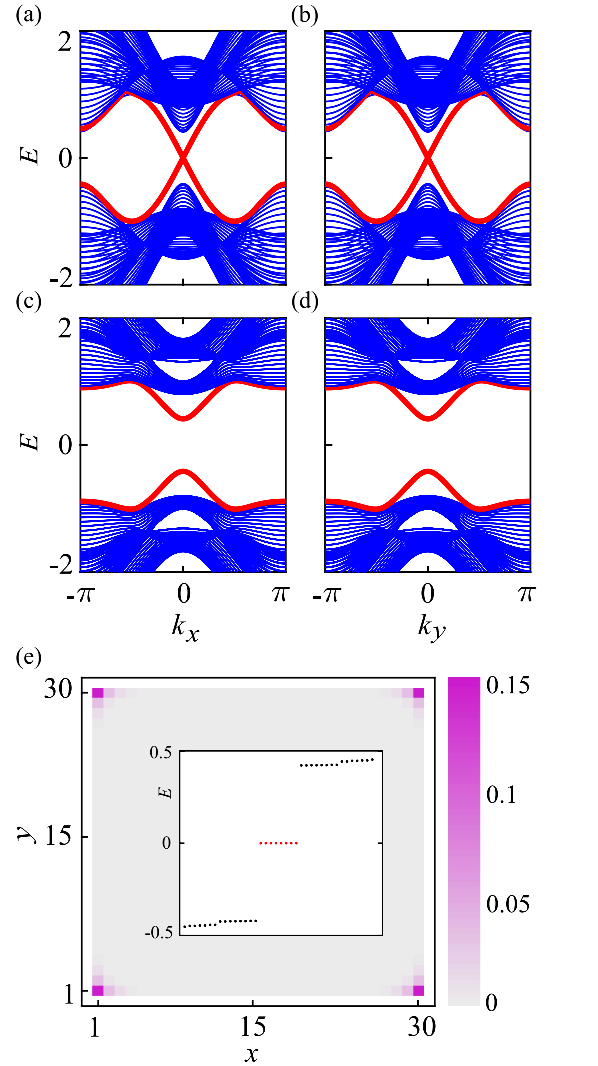

FIG. 2. Energy-band structure of a 2D magnetic TI nanoribbon along the (a) x and (b) y directions. The red curves in (a) and (b) denote two degenerate gapless chiral edge states. The zero-energy edge states exist at the $k_x = 0$ and $k_y = 0$ points, respectively. The BdG spectrum with a $d_{x^2-y^2}$-wave pairing along the (c) x and (d) y directions. In the presence of d-wave pairing, the edge states are gapped out (red curves). (e) The probability density distributions of the BdG wave functions with zero energies for a sample size with 30 × 30. There are two MBSs localized at each corner due to the mirror symmetry of the BdG Hamiltonian. The inset shows the eigenenergies of the same sample with energies around zero. Note that there are eight zero-energy modes in the gap shown as eight red dots. The parameters are chosen to be $m_0 = -0.8$, $\lambda_z = 0.4$, $\lambda_{so} = 1$, $m_x = m_y = 1$, $\mu = 0$, and $\Delta_1 = 0.5$.

$$U H_{\rm BdG} U^{-1} = \begin{pmatrix} H_+(\mathbf{k}) & 0 \\ 0 & H_-(\mathbf{k}) \end{pmatrix}, \tag{18}$$

where $H_+(\mathbf{k})$ acts on the $+i$ mirror subspace, $H_-(\mathbf{k})$ acts on the $-i$ mirror subspace, they are expressed as

$$\begin{aligned} H_\pm(\mathbf{k}) = {}& m(k)\eta_z\tau_z \pm \lambda_z\eta_z - \mu\tau_z + \Delta(k)\tau_x \\ & + \lambda_{so}[\sin(k_x)\eta_x \pm \sin(k_y)\eta_y]\tau_z, \end{aligned} \tag{19}$$

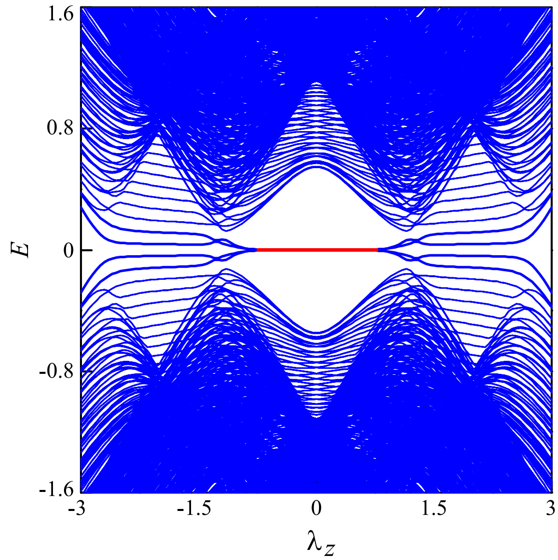

FIG. 3. BdG energy spectrum with open boundary conditions in the x and y directions as a function of λ_z. The sample size is 20×20. The red line corresponds to eightfold-degenerate MCSs, which exist only for finite amplitudes of the exchange field. The parameters are chosen to be $m_0 = -0.8$, $\lambda_{\rm so} = 1$, $m_x = m_y = 1$, $\mu = 0$, and $\Delta_1 = 0.5$.

and η_i are the Pauli matrices. Note that the similar mirror symmetries, in combination with time-reversal symmetry, were taken into account in topological crystalline superconductors [68].

In order to solve the effective Hamiltonian of the edge states, we consider the continuum model of the lattice Hamiltonian by expanding its wave vector $\mathbf{k}$ in Eqs. (18)–(19) to second order around the $\Gamma = (0,0)$ point (we can also expand $\mathbf{k}$ around the other high-symmetry points, e.g., M, which will not influence the discussions below).

$$H_c(\mathbf{k}) = \begin{pmatrix} H_+^c(\mathbf{k}) & 0 \\ 0 & H_-^c(\mathbf{k}) \end{pmatrix}, \tag{20}$$

where

$$H_\pm^c(\mathbf{k}) = \left[m_1 - \frac{1}{2}\left(m_x k_x^2 + m_y k_y^2\right)\right]\eta_z\tau_z \pm \lambda_z\eta_z - \mu\tau_z$$
$$+ \lambda_{\rm so}[k_x\eta_x \pm k_y\eta_y]\tau_z - \frac{\Delta_1}{2}\left(k_x^2 - k_y^2\right)\tau_x, \tag{21}$$

where $m_1 = m_0 + m_x + m_y$.

We first solve edge I of the four edges (see Fig. 1). By expressing k_y as $-i\partial_y$ and treating the pairing terms as perturbation (which is valid when the pairing amplitude is relatively small), we can rewrite the Hamiltonian $H_\pm^c$ as $H_\pm^c = H_\pm^1 + H_\pm^2$:

$$H_\pm^1(k_x, -i\partial_y) = \left(m_1 + m_y\partial_y^2/2\right)\eta_z\tau_z \pm \lambda_z\eta_z - \mu\tau_z$$
$$\mp i\lambda_{\rm so}\eta_y\tau_z\partial_y, \tag{22}$$

$$H_\pm^2(k_x, -i\partial_y) = \lambda_{\rm so}k_x\eta_x\tau_z - (\Delta_1/2)\tau_x\partial_y^2, \tag{23}$$

where we have already neglected the insignificant k_x^2 terms. To obtain the eigenvalue equation $H_\pm^1\phi_\pm(y) = E_\pm\phi_\pm(y)$, with $E_\pm = 0$ under boundary conditions $\phi_\pm(0) = \phi_\pm(+\infty) = 0$, we write the solution in the following form:

$$\phi_\pm(y) = \mathcal{N}_y \sin(\alpha y)e^{-\beta y}e^{ik_x x}\chi_\pm, \tag{24}$$

where the normalization constant $\mathcal{N}_y = 2\sqrt{\beta(\alpha^2+\beta^2)/\alpha^2}$. The eigenvector $\chi_\pm$ satisfies $\eta_x\chi_\pm = \mp\mathrm{sgn}(m_y)\chi_\pm$. For the sake of simplicity, we assume $\lambda_{\rm so} > 0$ in our discussions unless otherwise specified. Then the effective Hamiltonian for edge I can be obtained in this basis as

$$\mathcal{H}_\pm^{\rm I} = \int_0^{+\infty} \phi_\pm^*(y)H_\pm^2\phi_\pm(y)\,dy. \tag{25}$$

Therefore, we have

$$\mathcal{H}_\pm^{\rm I} = \mp\mathrm{sgn}(m_y)\lambda_{\rm so}k_x\tau_z + \frac{\Delta_1}{2}\left(\alpha_1^2+\beta_1^2\right)\tau_x, \tag{26}$$

where $\alpha_1^2 + \beta_1^2 = 2(m_1 \pm \lambda_z \pm \mu)/m_y$.

The effective Hamiltonian for edges II, III, and IV can be obtained by the same procedures:

$$\mathcal{H}_\pm^{\rm II} = \mp\mathrm{sgn}(m_x)\lambda_{\rm so}k_y\tau_z - \frac{\Delta_1}{2}\left(\alpha_2^2+\beta_2^2\right)\tau_x, \tag{27}$$

$$\mathcal{H}_\pm^{\rm III} = \pm\mathrm{sgn}(m_y)\lambda_{\rm so}k_x\tau_z + \frac{\Delta_1}{2}\left(\alpha_1^2+\beta_1^2\right)\tau_x, \tag{28}$$

$$\mathcal{H}_\pm^{\rm IV} = \pm\mathrm{sgn}(m_x)\lambda_{\rm so}k_y\tau_z - \frac{\Delta_1}{2}\left(\alpha_2^2+\beta_2^2\right)\tau_x, \tag{29}$$

where $\alpha_2^2 + \beta_2^2 = 2(m_1 \pm \lambda_z \pm \mu)/m_x$.

The first kinetic terms of the effective Hamiltonian in Eqs. (26)–(29) describe the gapless edge states, which are gapped out by the second terms with Dirac mass. Moreover, at the mirror subspace with the Hamiltonians H_+^i and H_-^i ($i = \mathrm{I} \sim \mathrm{IV}$), due to mirror-reflection symmetry, the Dirac mass terms change sign along four edges, edges I to IV, resulting from the

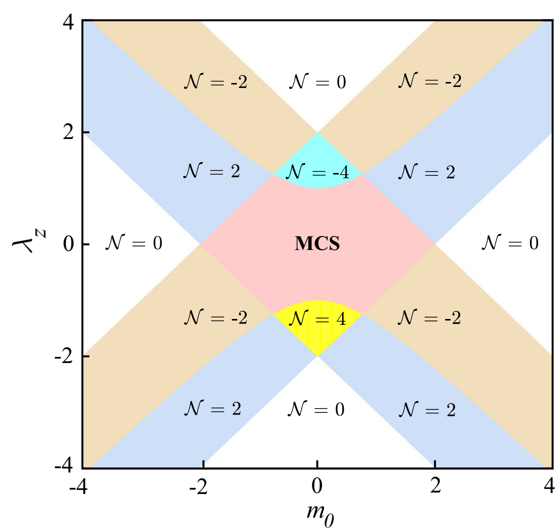

FIG. 4. Topological phase diagram of the magnetic TI/$d_{x^2-y^2}$ high-temperature superconductor hybrid system in the (m_0, λ_z) plane, which reveals three distinct phases: (i) second-order topological superconductor with MCSs, (ii) chiral MZMs characterized by a finite Chern number $\mathcal{N}$, and (iii) topologically trivial states $\mathcal{N} = 0$ with zero chiral MZMs and MCSs. The parameters are chosen to be $\lambda_{\rm so} = 1$, $m_x = m_y = 1$, $\mu = 0$, and $\Delta_1 = 0.5$.

$d_{x^2-y^2}$ pairing symmetry; that is, any two adjacent edge states have opposite Dirac masses, while the same signs occur for the first kinetic terms along the anticlockwise direction of the edges. As a result, there is one MBS at each corner of a square sample within each mirror subspace of the Hamiltonian (see the Jackiw-Rebbi model [69]), i.e., two MBSs at each corner. By comparing the coefficients of the Dirac mass terms, containing $\alpha_1^2+\beta_1^2$ and $\alpha_2^2+\beta_2^2$, for the two adjacent edge states in Eqs. (26)–(29), in order to ensure the existence of Majorana corner states, m_x and m_y should satisfy the relation $m_x m_y > 0$. Note that the BdG system supports two MCSs at each corner in the whole regime of the second-order topological phase considered here due to the mirror-reflection symmetry $\mathcal{M}_z$ for the Hamiltonian $H_{\rm BdG}(\mathbf{k})$. When this mirror-reflection symmetry is broken, a single MCS at each corner can be achieved (see the Appendix).

B. $s_\pm$-wave pairing

Here, we consider the magnetic TI approximated by an $s_\pm$ superconducting pairing, which is relevant for iron-based high-temperature superconductors [62–66]. The pairing amplitude of an $s_\pm$-wave superconductor satisfies

$$\Delta_x = \Delta_y = \Delta_2. \tag{30}$$

As in the case for a d-wave superconductor, we first consider the energy-band spectrum of the system. Figures 5(a) and 5(b) show the energy-band structure of a 2D magnetic TI nanoribbon along the x and y directions, respectively. But, in contrast to the case for hybrid systems of magnetic TI/d-wave superconductors, the zero-energy edge states in the y and x directions exist at the $k_x=0$ and $k_y=\pi$ points for magnetic TI/$s_\pm$-wave superconductor hybrid systems when m_y is set to a negative value. In the presence of the $s_\pm$ pairing, the edges are gapped out [see the red curves in Figs. 5(c) and 5(d)], where the hybrid system enters the topologically trivial regime. However, similar to the case for a d-wave superconductor, each corner of the finite-size sample supports two localized MBSs [see Fig. 5(e)]. Moreover, when m_y is set to have the same sign as m_x, there are no MCSs. Note that the system may support a single MCS at each corner when the mirror-reflection symmetry $\mathcal{M}_z$ is broken (see the Appendix).

In order to understand the existence of MCSs with $s_\pm$-wave pairing, we also consider the edge theory. In this part, we consider the continuum model of the lattice Hamiltonian by expanding its wave vector $\mathbf{k}$ in Eqs. (18) and (19) to second order around the $X=(0,\pi)$ point of the Brillouin zone, obtaining

$$H_c(\mathbf{k}) = \begin{pmatrix} H_+^c(\mathbf{k}) & 0 \\ 0 & H_-^c(\mathbf{k}) \end{pmatrix}, \tag{31}$$

where

$$\begin{aligned} H_\pm^c(\mathbf{k}) &= \left[m_2 - \frac{1}{2}\left(m_x k_x^2 - m_y k_y^2\right)\right]\eta_z\tau_z \pm \lambda_z\eta_z \\ &+ \lambda_{\rm so}[k_x\eta_x \pm k_y\eta_y]\tau_z - \mu\tau_z \\ &+ \left[\Delta_0 - \frac{\Delta_2}{2}\left(k_x^2 - k_y^2\right)\right]\tau_x \end{aligned} \tag{32}$$

and $m_2 = m_0 + m_x - m_y$.

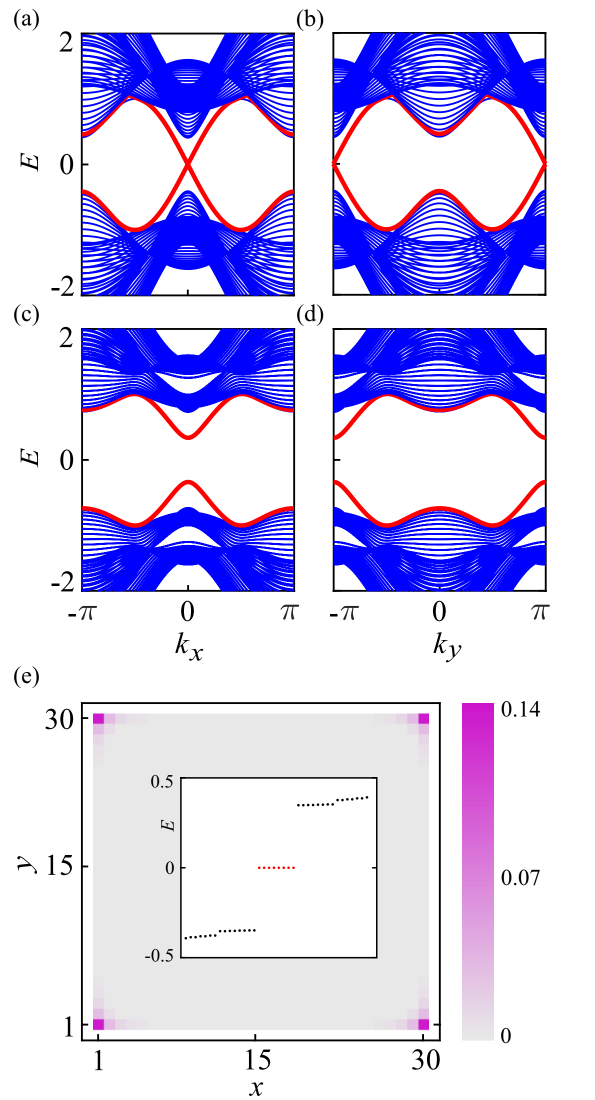

FIG. 5. Energy-band structure of a 2D magnetic TI nanoribbon along the (a) x and (b) y directions. The red curves in (a) and (b) denote two degenerate gapless chiral edge states. The zero-energy edge states exist at the $k_x=0$ and $k_y=\pi$ points, respectively. The BdG spectrum with an $s_\pm$-wave pairing along the (c) x and (d) y directions. In the presence of $s_\pm$-wave pairing, the edge states are gapped out (red curves). (e) The probability density distributions of BdG wave functions with zero energies for a sample of size 30×30. There are two MBSs localized at each corner due to the mirror symmetry of the BdG Hamiltonian. The inset shows eigenenergies of the same sample with energies around zero. Note that there are eight zero-energy modes in the gap shown as eight red dots. The parameters are chosen to be $m_0=-0.8$, $\lambda_z=0.4$, $\lambda_{\rm so}=1$, $m_x=-m_y=1$, $\mu=0$, $\Delta_0=0$, and $\Delta_2=0.4$.

Then, the effective Hamiltonian for edges I, II, III, and IV can be obtained as

$$\mathcal{H}_\pm^{\rm I} = \mp{\rm sgn}(m_y)\lambda_{\rm so}k_x\tau_z + \left[\Delta_0 + \frac{\Delta_2}{2}\left(\alpha_3^2+\beta_3^2\right)\right]\tau_x, \tag{33}$$

$$\mathcal{H}_\pm^{\rm II} = \pm{\rm sgn}(m_x)\lambda_{\rm so}k_y\tau_z + \left[\Delta_0 - \frac{\Delta_2}{2}\left(\alpha_4^2+\beta_4^2\right)\right]\tau_x, \tag{34}$$

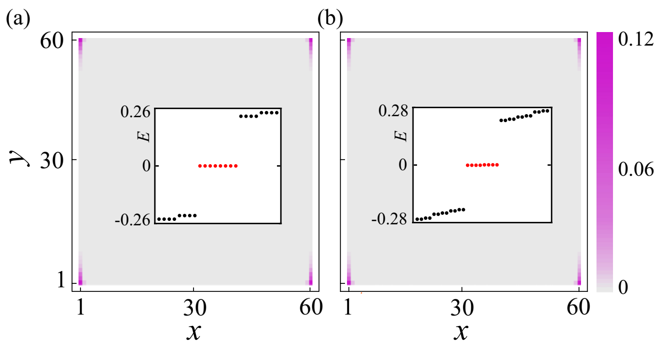

FIG. 6. The probability density distributions (with the scale shown in the right vertical bar) of the BdG wave functions with zero energies for a sample size of 60×60, with different chemical potentials: (a) $\mu = 0$ and (b) $\mu = 0.1$. There are two MBSs localized at each corner. A finite chemical potential μ will not destroy the MCSs. The inset shows the eigenenergies of the same sample with the energies around zero. Note that there are eight zero-energy modes in the gap shown as eight red dots. Other parameters are chosen to be $m_0 = -0.8$, $\lambda_z = 0.1$, $\lambda_{\rm so} = 1$, $m_x = -m_y = 1$, $\Delta_0/\Delta_2 = 0.6$, and $\Delta_2 = 0.4$.

$$\mathcal{H}_{\pm}^{\rm III} = \pm{\rm sgn}(m_y)\lambda_{\rm so}k_x\tau_z + \left[\Delta_0 + \frac{\Delta_2}{2}\left(\alpha_3^2 + \beta_3^2\right)\right]\tau_x, \quad (35)$$

$$\mathcal{H}_{\pm}^{\rm IV} = \mp{\rm sgn}(m_x)\lambda_{\rm so}k_y\tau_z + \left[\Delta_0 - \frac{\Delta_2}{2}\left(\alpha_4^2 + \beta_4^2\right)\right]\tau_x, \quad (36)$$

where $\alpha_3^2 + \beta_3^2 = -2(m_2 \pm \lambda_z \pm \mu)/m_y$ and $\alpha_4^2 + \beta_4^2 = 2(m_2 \pm \lambda_z \pm \mu)/m_x$.

First, according to Eqs. (33)–(36), in contrast to the case of d-wave superconductors, the existence of Majorana corner states requires m_x and m_y to satisfy $m_x m_y < 0$ for hybrid systems with $s_\pm$ superconducting pairing.

Second, within each mirror subspace of the BdG Hamiltonian, in order to ensure the opposite Dirac mass terms for any two gapped adjacent edge states, the following criterion should be satisfied:

$$\left[\Delta_0 + \frac{\Delta_2}{2}\left(\alpha_3^2 + \beta_3^2\right)\right]\left[\Delta_0 - \frac{\Delta_2}{2}\left(\alpha_4^2 + \beta_4^2\right)\right] < 0. \quad (37)$$

Therefore, we have

$$\left[\frac{\Delta_0}{\Delta_2} - \frac{m_2 \pm \lambda_z \pm \mu}{m_y}\right]\left[\frac{\Delta_0}{\Delta_2} - \frac{m_2 \pm \lambda_z \pm \mu}{m_x}\right] < 0. \quad (38)$$

Equations (13) and (38) determine the system parameters, including the pairing amplitude and magnetic exchange interaction, required for the existence of MCSs for $s_\pm$ superconducting pairing. As an example, according to Eqs. (13) and (38), the criterion of $\Delta_0/\Delta_2 < 1$ should be satisfied to ensure the existence of MCSs within each mirror subspace of the Hamiltonian if $m_0 = -1$ and $m_x = -m_y = -1$.

Figure 6(a) shows the emergence of MCSs by computing the probability density distribution of the BdG wave functions for the magnetic TI/$s_\pm$ superconductor hybrid system with the parameters λ_z, Δ_0, Δ_2, m_x, and m_y satisfying all of these criteria. There are then two MBSs localized at each corner. A finite chemical potential μ within the limit of Eq. (38) will not destroy the MCSs, as shown in Fig. 6(b).

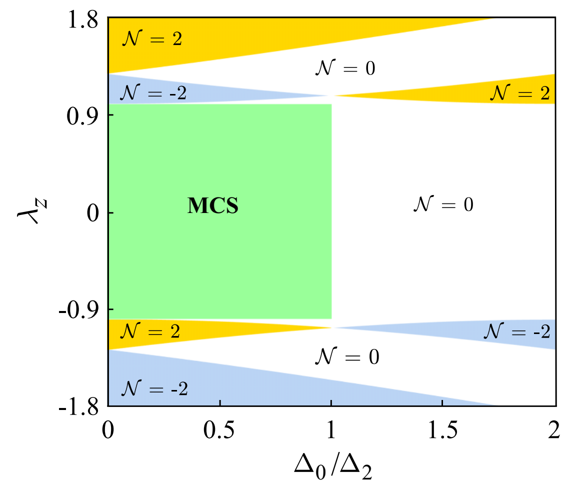

FIG. 7. Topological phase diagram of a magnetic TI/$s_\pm$ high-temperature superconductor hybrid system in the $(\lambda_z, \Delta_0/\Delta_2)$ plane, which reveals three distinct phases: (i) second-order topological superconductor with MCSs, (ii) chiral MZMs characterized by a finite Chern number $\mathcal{N}$, and (iii) topologically trivial states $\mathcal{N} = 0$ with zero chiral MZMs and MCSs. Recall that $\Delta_x = \Delta_y = \Delta_2$, as shown in Eq. (30). The parameters are chosen to be $m_0 = -1$, $\lambda_{\rm so} = 1$, $m_x = -m_y = 1$, $\mu = 0$, and $\Delta_2 = 0.4$.

In terms of topological phase diagram, parts of the phase boundaries are determined by the zero eigenenergy of the BdG Hamiltonian in Eq. (5) at the four corners of the Brillouin zone of a square lattice, i.e., $\varGamma = (0, 0)$, $X = (0, \pi)$, $Y = (\pi, 0)$, and $M = (\pi, \pi)$. The energies for a TI/$s_\pm$ hybrid system at these points are

$$E_\varGamma = \pm\sqrt{(\mu \mp m_0 \mp m_x \mp m_y)^2 + (\Delta_0 + 2\Delta_2)^2} \pm \lambda_z, \quad (39)$$

$$E_M = \pm\sqrt{(\mu \pm m_0 \mp m_x \mp m_y)^2 + (\Delta_0 - 2\Delta_2)^2} \pm \lambda_z, \quad (40)$$

$$E_X = \pm\sqrt{(\mu \pm m_0 \pm m_x \mp m_y)^2 + \Delta_0^2} \pm \lambda_z, \quad (41)$$

$$E_Y = \pm\sqrt{(\mu \mp m_0 \pm m_x \mp m_y)^2 + \Delta_0^2} \pm \lambda_z. \quad (42)$$

In addition, the phase boundaries are simultaneously determined by Eqs. (13) and (38). Figure 7 shows the topological phase diagram of the magnetic TI/$s_\pm$ high-temperature superconductor hybrid system in the $(\lambda_z, \Delta_0/\Delta_2)$ plane. As in the case of d-wave superconductors, there are three distinct phases: (i) a second-order topological superconductor with MCSs, (ii) chiral MZMs characterized by a finite Chern number $\mathcal{N}$, and (iii) topologically trivial states $\mathcal{N} = 0$ with zero chiral MZMs and MCSs.

IV. DISCUSSION AND CONCLUSION

For experimental realizations, we require a magnetic TI in proximity to a high-temperature superconductor. For the magnetic TI, we can consider the recently experimentally discovered TIs of 2D transition-metal dichalcogenides (e.g., monolayer WTe_2 [70,71]) or IV-VI semiconductors (e.g., monolayer PbS [72,73]), which coat a ferromagnetic insulator. The high-temperature superconductors could be cuprate-based [59–61] or iron-based [64,66] materials, where topological superconductivity has been experimentally reported. It is thus quite attractive to study second-order TSC and possibly observe MCSs in these systems by considering their hybrids. Moreover, the magnetic exchange interaction in magnetic TI is usually highly tunable by external fields, and thus, it is also interesting to study how the exchange interaction influences the features of second-order topological superconductivity.

In conclusion, we investigated the hybrid structure of a magnetic TI and a high-temperature superconductor, which exhibits second-order topological superconductivity. Both d-wave and $s_{\pm}$-wave superconducting pairings related to high-temperature superconductors were discussed. The hybrid systems are in the topologically trivial regime but still support MBSs at each corner of a square sample. Because the hybrid systems preserve mirror-reflection symmetry, there are two MBSs at each corner in the whole regime of the second-order topological phase studied here. We derived their corresponding topological phase diagrams, which emphasize the role of magnetic exchange interactions and pairing amplitudes. An intuitive edge argument showed that the corner states result from the opposite Dirac masses of two adjacent edges due to pairing symmetry. In the future, it would be interesting to look for experimental realizations of second-order TSCs and study the possibility of non-Abelian braiding of MCSs in a 2D system.

ACKNOWLEDGMENTS

T.L. acknowledges support from a JSPS Postdoctoral Fellowship (P18023). F.N. is supported in part by the MURI Center for Dynamic Magneto-Optics via the Air Force Office of Scientific Research (AFOSR; Grant No. FA9550-14-1-0040), Army Research Office (ARO; Grant No. W911NF-18-1-0358), Asian Office of Aerospace Research and Development (AOARD; Grant No. FA2386-18-1-4045), Japan Science and Technology Agency (JST; the ImPACT program and CREST Grant No. JPMJCR1676), Japan Society for the Promotion of Science (JSPS; JSPS-RFBR Grant No. 17-52-50023 and JSPS-FWO Grant No. VS.059.18N), the RIKEN-AIST Challenge Research Fund, and the John Templeton Foundation.

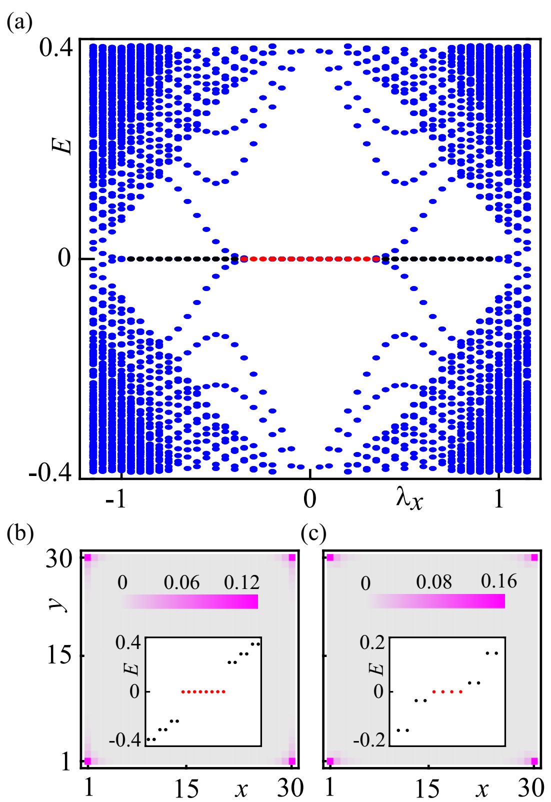

FIG. 8. (a) BdG energy spectra of a $d_{x^2-y^2}$-wave pairing superconductor with open boundaries along the x and y directions as a function of λ_x. The red dots denote eightfold-degenerate MCSs, and the black dots represent the fourfold-degenerate MCSs. The probability density distributions of mid-gap states for (b) $\lambda_x = 0.3$ and (c) $\lambda_x = 0.5$. The inset shows the eigenenergies with energies around zero. The parameters are chosen to be $m_0 = -0.8$, $\lambda_z = 0.4$, $\lambda_{so} = 1$, $m_x = m_y = 1$, $\mu = 0$, and $\Delta_1 = 0.5$.

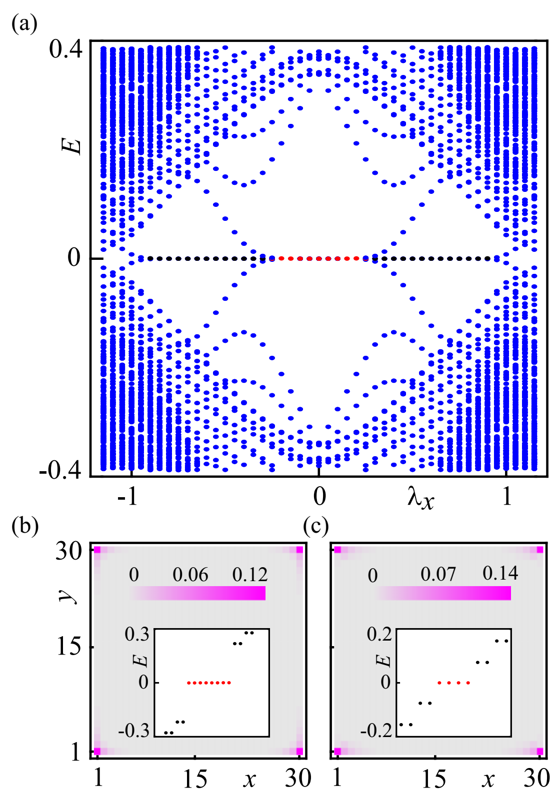

FIG. 9. (a) BdG energy spectra of an $s_{\pm}$-wave pairing superconductor with open boundaries along the x and y directions as a function of λ_x. The red dots denote eightfold-degenerate MCSs, and the black dots represent the fourfold-degenerate MCSs. The probability density distributions of mid-gap states for (b) $\lambda_x = 0.2$ and (c) $\lambda_x = 0.5$. The inset shows the eigenenergies with energies around zero. The parameters are chosen to be $m_0 = -0.8$, $\lambda_z = 0.4$, $\lambda_{so} = 1$, $m_x = -m_y = 1$, $\mu = 0$, $\Delta_0 = 0$, and $\Delta_2 = 0.4$.

APPENDIX: BROKEN MIRROR-REFLECTION SYMMETRY

The Hamiltonian $H_{\rm BdG}(\mathbf{k})$ in Eq. (5) respects the mirror-reflection symmetry $\mathcal{M}_z$. Therefore, there are two MCSs at each corner in the whole regime of the second-order topological phase considered here. When this mirror-reflection symmetry is broken, a single MCS at each corner may be achieved for both d-wave and $s_\pm$-wave superconducting hybrid systems.

Let us now break the mirror-reflection symmetry by adding the term $\lambda_x s_x$ to Eq. (5), so the Hamiltonian becomes

$$\bar{H}_{\rm BdG}(\mathbf{k}) = m(k)\sigma_z\tau_z + \lambda_{\rm so}[\sin(k_x)s_x + \sin(k_y)s_y]\sigma_x\tau_z + \lambda_z s_z - \mu\tau_z + \Delta(k)\tau_x + \lambda_x s_x. \quad \text{(A1)}$$

In the presence of the $\lambda_x s_x$ term, the mirror-reflection symmetry is broken. Figure 8(a) shows the BdG energy spectrum of a $d_{x^2-y^2}$-wave pairing superconducting hybrid system with open boundaries along the x and y directions as a function of λ_x. The eightfold-degenerate MCSs exist [see red dots in Fig. 8(a) and probability density distributions in Fig. 8(c)] when λ_x is small, while there are only fourfold-degenerate MCSs [see black dots in Fig. 8(b) and probability density distributions Fig. 8(c)] as λ_x increases, where the second-order topological phase transition occurs. Therefore, a single MCS appears when the mirror reflection is broken with an appropriate magnitude of λ_x

As in the case for a d-wave superconductor, for a hybrid system with an $s_\pm$-wave pairing superconducting hybrid system, a single MCS at each corner can exist when the mirror-reflection symmetry is broken in the presence of the $\lambda_x s_x$ term with an appropriate magnitude (see Fig. 9). The effect of the breakdown of mirror-reflection symmetry on the MCSs in both d-wave and $s_\pm$-wave superconducting hybrid systems can be interpreted by considering the effective edge Hamiltonians derived from the Hamiltonian $\bar{H}_{\rm BdG}(\mathbf{k})$ in Eq. (A1), as treated based on the block-diagonal Hamiltonian [see Eqs. (18)–(29) and (31)–(38)].

[1] M. Z. Hasan and C. L. Kane, Colloquium: Topological insulators, Rev. Mod. Phys. **82**, 3045 (2010).

[2] X. L. Qi and S. C. Zhang, Topological insulators and superconductors, Rev. Mod. Phys. **83**, 1057 (2011).

[3] J. Alicea, New directions in the pursuit of Majorana fermions in solid state systems, Rep. Prog. Phys. **75**, 076501 (2012).

[4] C. W. J. Beenakker, Search for Majorana fermions in superconductors, Annu. Rev. Condens. Matter Phys. **4**, 113 (2013).

[5] M. Sato and Y. Ando, Topological superconductors: A review, Rep. Prog. Phys. **80**, 076501 (2017).

[6] R. Aguado, Majorana quasiparticles in condensed matter, La Rivista del Nuovo Cimento **40**, 523 (2017).

[7] C. Nayak, S. H. Simon, A. Stern, M. Freedman, and S. Das Sarma, Non-Abelian anyons and topological quantum computation, Rev. Mod. Phys. **80**, 1083 (2008).

[8] J. Alicea, Y. Oreg, G. Refael, F. von Oppen, and M. P. A. Fisher, Non-Abelian statistics and topological quantum information processing in 1D wire networks, Nat. Phys. **7**, 412 (2011).

[9] S. D. Sarma, M. Freedman, and C. Nayak, Majorana zero modes and topological quantum computation, npj Quantum Inf. **1**, 15001 (2015).

[10] Y. Oreg, G. Refael, and F. von Oppen, Helical Liquids and Majorana Bound States in Quantum Wires, Phys. Rev. Lett. **105**, 177002 (2010).

[11] R. M. Lutchyn, J. D. Sau, and S. Das Sarma, Majorana Fermions and a Topological Phase Transition in Semiconductor-Superconductor Heterostructures, Phys. Rev. Lett. **105**, 077001 (2010).

[12] V. Mourik, K. Zuo, S. M. Frolov, S. R. Plissard, E. P. A. M. Bakkers, and L. P. Kouwenhoven, Signatures of Majorana fermions in hybrid superconductor-semiconductor nanowire devices, Science **336**, 1003 (2012).

[13] M. T. Deng, S. Vaitiekenas, E. B. Hansen, J. Danon, M. Leijnse, K. Flensberg, J. Nygård, P. Krogstrup, and C. M. Marcus, Majorana bound state in a coupled quantum-dot hybrid-nanowire system, Science **354**, 1557 (2016).

[14] H. Zhang, C. X. Liu, S. Gazibegovic, D. Xu, J. A. Logan, G. Wang, N. van Loo, J. D. S. Bommer, M. W. A. de Moor, D. Car, R. L. M. Op het Veld, P. J. van Veldhoven, S. Koelling, M. A. Verheijen, M. Pendharkar, D. J. Pennachio, B. Shojaei, J. S. Lee, C. J. Palmstrøm, E. P. A. M. Bakkers, S. D. Sarma, and L. P. Kouwenhoven, Quantized Majorana conductance, Nature (London) **556**, 74 (2018).

[15] Ö. Gül, H. Zhang, J. D. S. Bommer, M. W. A. de Moor, D. Car, S. R. Plissard, E. P. A. M. Bakkers, A. Geresdi, K. Watanabe, T. Taniguchi, and L. P. Kouwenhoven, Ballistic Majorana nanowire devices, Nat. Nanotechnol. **13**, 192 (2018).

[16] B. Braunecker and P. Simon, Interplay between Classical Magnetic Moments and Superconductivity in Quantum One-Dimensional Conductors: Toward a Self-Sustained Topological Majorana Phase, Phys. Rev. Lett. **111**, 147202 (2013).

[17] J. Klinovaja, P. Stano, A. Yazdani, and D. Loss, Topological Superconductivity and Majorana Fermions in RKKY Systems, Phys. Rev. Lett. **111**, 186805 (2013).

[18] S. Nadj-Perge, I. K. Drozdov, J. Li, H. Chen, S. Jeon, J. Seo, A. H. MacDonald, B. A. Bernevig, and A. Yazdani, Observation of Majorana fermions in ferromagnetic atomic chains on a superconductor, Science **346**, 602 (2014).

[19] R. Pawlak, M. Kisiel, J. Klinovaja, T. Meier, S. Kawai, T. Glatzel, D. Loss, and E. Meyer, Probing atomic structure and Majorana wavefunctions in mono-atomic Fe chains on superconducting Pb surface, Npj Quantum Inf. **2**, 16035 (2016).

[20] L. Fu and C. L. Kane, Superconducting Proximity Effect and Majorana Fermions at the Surface of a Topological Insulator, Phys. Rev. Lett. **100**, 096407 (2008).

[21] J. D. Sau, R. M. Lutchyn, S. Tewari, and S. Das Sarma, Generic New Platform for Topological Quantum Computation Using Semiconductor Heterostructures, Phys. Rev. Lett. **104**, 040502 (2010).

[22] R. S. Akzyanov, A. L. Rakhmanov, A. V. Rozhkov, and F. Nori, Majorana fermions at the edge of superconducting islands, Phys. Rev. B **92**, 075432 (2015).

[23] R. S. Akzyanov, A. L. Rakhmanov, A. V. Rozhkov, and F. Nori, Tunable Majorana fermion from Landau quantization in 2D topological superconductors, Phys. Rev. B **94**, 125428 (2016).

[24] Q. L. He, L. Pan, A. L. Stern, E. C. Burks, X. Che, G. Yin, J. Wang, B. Lian, Q. Zhou, E. S. Choi, K. Murata, X. Kou, Z. Chen, T. Nie, Q. Shao, Y. Fan, S. C. Zhang, K. Liu, J. Xia, and K. L. Wang, Chiral Majorana fermion modes in a quantum anomalous Hall insulator–superconductor structure, Science **357**, 294 (2017).

[25] Y. Tanaka, T. Yokoyama, and N. Nagaosa, Manipulation of the Majorana Fermion, Andreev Reflection, and Josephson Current on Topological Insulators, Phys. Rev. Lett. **103**, 107002 (2009).

[26] J. Linder, Y. Tanaka, T. Yokoyama, A. Sudbø, and N. Nagaosa, Unconventional Superconductivity on a Topological Insulator, Phys. Rev. Lett. **104**, 067001 (2010).

[27] F. Zhang, C. L. Kane, and E. J. Mele, Time-Reversal-Invariant Topological Superconductivity and Majorana Kramers Pairs, Phys. Rev. Lett. **111**, 056402 (2013).

[28] L. Ortiz, S. Varona, O. Viyuela, and M. A. Martin-Delgado, Localization and oscillations of Majorana fermions in a two-dimensional electron gas coupled with d-wave superconductors, Phys. Rev. B **97**, 064501 (2018).

[29] O. Viyuela, L. Fu, and M. A. Martin-Delgado, Chiral Topological Superconductors Enhanced by Long-Range Interactions, Phys. Rev. Lett. **120**, 017001 (2018).

[30] F. Zhang, C. L. Kane, and E. J. Mele, Surface State Magnetization and Chiral Edge States on Topological Insulators, Phys. Rev. Lett. **110**, 046404 (2013).

[31] W. A. Benalcazar, B. A. Bernevig, and T. L. Hughes, Quantized electric multipole insulators, Science **357**, 61 (2017).

[32] W. A. Benalcazar, B. A. Bernevig, and T. L. Hughes, Electric multipole moments, topological multipole moment pumping, and chiral hinge states in crystalline insulators, Phys. Rev. B **96**, 245115 (2017).

[33] J. Langbehn, Y. Peng, L. Trifunovic, F. von Oppen, and P. W. Brouwer, Reflection-Symmetric Second-Order Topological Insulators and Superconductors, Phys. Rev. Lett. **119**, 246401 (2017).

[34] Z. Song, Z. Fang, and C. Fang, $(d-2)$-Dimensional Edge States of Rotation Symmetry Protected Topological states, Phys. Rev. Lett. **119**, 246402 (2017).

[35] F. Schindler, A. M. Cook, M. G. Vergniory, Z. Wang, S. S. P. Parkin, B. A. Bernevig, and T. Neupert, Higher-order topological insulators, Sci. Adv. **4**, eaat0346 (2018).

[36] M. Ezawa, Higher-Order Topological Insulators and Semimetals on the Breathing Kagome and Pyrochlore Lattices, Phys. Rev. Lett. **120**, 026801 (2018).

[37] E. Khalaf, Higher-order topological insulators and superconductors protected by inversion symmetry, Phys. Rev. B **97**, 205136 (2018).

[38] M. Geier, L. Trifunovic, M. Hoskam, and P. W. Brouwer, Second-order topological insulators and superconductors with an order-two crystalline symmetry, Phys. Rev. B **97**, 205135 (2018).

[39] S. Imhof, C. Berger, F. Bayer, J. Brehm, L. W. Molenkamp, T. Kiessling, F. Schindler, C. H. Lee, M. Greiter, T. Neupert, and R. Thomale, Topolectrical-circuit realization of topological corner modes, Nat. Phys. **14**, 925 (2018).

[40] F. Schindler, Z. Wang, M. G. Vergniory, A. M. Cook, A. Murani, S. Sengupta, A. Y. Kasumov, R. Deblock, S. J. I. Drozdov, H. Bouchiat, S. Guéron, A. Yazdani, B. A. Bernevig, and T. Neupert, Higher-order topology in bismuth, Nat. Phys. **14**, 918 (2018).

[41] S. Franca, J. van den Brink, and I. C. Fulga, An anomalous higher-order topological insulator, Phys. Rev. B **98**, 201114(R) (2018).

[42] Z. Yan, F. Song, and Z. Wang, Majorana Corner Modes in a High-Temperature Platform, Phys. Rev. Lett. **121**, 096803 (2018).

[43] Q. Wang, C.-C. Liu, Y.-M. Lu, and F. Zhang, High-Temperature Majorana Corner States, Phys. Rev. Lett. **121**, 186801 (2018).

[44] C.-H. Hsu, P. Stano, J. Klinovaja, and D. Loss, Majorana Kramers Pairs in Higher-Order Topological Insulators, Phys. Rev. Lett. **121**, 196801 (2018).

[45] X. Zhu, Tunable Majorana corner states in a two-dimensional second-order topological superconductor induced by magnetic fields, Phys. Rev. B **97**, 205134 (2018).

[46] V. Dwivedi, C. Hickey, T. Eschmann, and S. Trebst, Majorana corner modes in a second-order Kitaev spin liquid, Phys. Rev. B **98**, 054432 (2018).

[47] Y. Wang, M. Lin, and T. L. Hughes, Weak-pairing higher order topological superconductors, Phys. Rev. B **98**, 165144 (2018).

[48] C. X. Liu, X. L. Qi, X. Dai, Z. Fang, and S. C. Zhang, Quantum Anomalous Hall Effect in $Hg_{1-y}Mn_yTe$ Quantum Wells, Phys. Rev. Lett. **101**, 146802 (2008).

[49] J. Wang, B. Lian, H. Zhang, Y. Xu, and S. C. Zhang, Quantum Anomalous Hall Effect with Higher Plateaus, Phys. Rev. Lett. **111**, 136801 (2013).

[50] R. Yu, W. Zhang, H. J. Zhang, S. C. Zhang, X. Dai, and Z. Fang, Quantized anomalous Hall effect in magnetic topological insulators, Science **329**, 61 (2010).

[51] I. Lee, C. K. Kim, J. Lee, S. J. L. Billinge, R. Zhong, J. A. Schneeloch, T. Liu, T. Valla, J. M. Tranquada, G. Gu, and J. C. S. Davis, Imaging Dirac-mass disorder from magnetic dopant atoms in the ferromagnetic topological insulator $Cr_x(Bi_{0.1}Sb_{0.9})_{2-x}Te_3$, Proc. Natl. Acad. Sci. U.S.A. **112**, 1316 (2015).

[52] C. Z. Chang, J. Zhang, Xi. Feng, J. Shen, Z. Zhang, M. Guo, K. Li, Y. Ou, P. Wei, L. L. Wang, Z. Q. Ji, Y. Feng, S. Ji, X. Chen, J. Jia, X. Dai, Z. Fang, S. C. Zhang, K. He, Y. Wang, L. Lu, X. C. Ma, and Q. K. Xue, Experimental observation of the quantum anomalous Hall effect in a magnetic topological insulator, Science **340**, 167 (2013).

[53] M. Mogi, M. Kawamura, A. Tsukazaki, R. Yoshimi, K. S. Takahashi, M. Kawasaki, and Y. Tokura, Tailoring tricolor structure of magnetic topological insulator for robust axion insulator, Sci. Adv. **3**, 1 (2017).

[54] Y. Fan, P. Upadhyaya, X. Kou, M. Lang, S. Takei, Z. Wang, J. Tang, Li. He, L. T. Chang, M. Montazeri, G. Yu, W. Jiang, T. Nie, R. N. Schwartz, Y. Tserkovnyak, and K. L. Wang, Magnetization switching through giant spin-orbit torque in a magnetically doped topological insulator heterostructure, Nat. Mater. **13**, 699 (2014).

[55] J. G. Checkelsky, J. Ye, Y. Onose, Y. Iwasa, and Y. Tokura, Dirac-fermion-mediated ferromagnetism in a topological insulator, Nat. Phys. **8**, 729 (2012).

[56] C. Z. Chang, W. Zhao, D. Y. Kim, H. Zhang, B. A. Assaf, D. Heiman, S. C. Zhang, C. Liu, M. H. W. Chan, and J. S. Moodera, High-precision realization of robust quantum anomalous Hall state in a hard ferromagnetic topological insulator, Nat. Mater. **14**, 473 (2015).

[57] C. Z. Chang and M. Li, Quantum anomalous Hall effect in time-reversal-symmetry breaking topological

insulators, J. Phys.: Condens. Matter **28**, 123002 (2016).

[58] P. Wei, F. Katmis, B. A. Assaf, H. Steinberg, P. Jarillo-Herrero, D. Heiman, and J. S. Moodera, Exchange-Coupling-Induced Symmetry Breaking in Topological Insulators, Phys. Rev. Lett. **110**, 186807 (2013).

[59] P. Zareapour, A. Hayat, S. Y. F. Zhao, M. Kreshchuk, A. Jain, D. C. Kwok, Na. Lee, S. W. Cheong, Z. Xu, A. Yang, G. D. Gu, S. Jia, R. J. Cava, and K. S. Burch, Proximity-induced high-temperature superconductivity in the topological insulators Bi_2Se_3 and Bi_2Te_3, Nat. Commun. **3**, 1056 (2012).

[60] Z. X. Li, C. Chan, and H. Yao, Realizing Majorana zero modes by proximity effect between topological insulators and d-wave high-temperature superconductors, Phys. Rev. B **91**, 235143 (2015).

[61] E. Wang, H. Ding, A. V. Fedorov, W. Yao, Z. Li, Y. F. Lv, K. Zhao, L. G. Zhang, Z. Xu, J. Schneeloch, R. Zhong, S. H. Ji, L. Wang, K. He, X. Ma, G. Gu, H. Yao, Q. K. Xue, X. Chen, and S. Zhou, Fully gapped topological surface states in Bi_2Se_3 films induced by a d-wave high-temperature superconductor, Nat. Phys. **9**, 621 (2013).

[62] G. R. Stewart, Superconductivity in iron compounds, Rev. Mod. Phys. **83**, 1589 (2011).

[63] G. Xu, B. Lian, P. Tang, X. L. Qi, and S. C. Zhang, Topological Superconductivity on the Surface of Fe-Based Superconductors, Phys. Rev. Lett. **117**, 047001 (2016).

[64] D. Wang, L. Kong, P. Fan, H. Chen, S. Zhu, W. Liu, L. Cao, Y. Sun, S. Du, J. Schneeloch, R. Zhong, G. Gu, L. Fu, H. Ding, and H.-J. Gao, Evidence for Majorana bound state in an iron-based superconductor, Science **362**, 333 (2018).

[65] P. J. Hirschfeld, M. M. Korshunov, and I. I. Mazin, Gap symmetry and structure of Fe-based superconductors, Rep. Prog. Phys. **74**, 124508 (2011).

[66] P. Zhang, K. Yaji, T. Hashimoto, Y. Ota, T. Kondo, K. Okazaki, Z. Wang, J. Wen, G. D. Gu, H. Ding, and S. Shin, Observation of topological superconductivity on the surface of an iron-based superconductor, Science **360**, 182 (2018).

[67] C. Z. Chen, Y. M. Xie, J. Liu, P. A. Lee, and K. T. Law, Quasi-one-dimensional quantum anomalous Hall systems as new platforms for scalable topological quantum computation, Phys. Rev. B **97**, 104504 (2018).

[68] F. Zhang, C. L. Kane, and E. J. Mele, Topological Mirror Superconductivity, Phys. Rev. Lett. **111**, 056403 (2013).

[69] R. Jackiw and C. Rebbi, Solitons with fermion number 1/2, Phys. Rev. D **13**, 3398 (1976).

[70] S. Wu, V. Fatemi, Q. D. Gibson, K. Watanabe, T. Taniguchi, R. J. Cava, and P. Jarillo-Herrero, Observation of the quantum spin Hall effect up to 100 Kelvin in a monolayer crystal, Science **359**, 76 (2018).

[71] X. Qian, J. Liu, L. Fu, and J. Li, Quantum spin Hall effect in two-dimensional transition metal dichalcogenides, Science **346**, 1344 (2014).

[72] W. Wan, Y. Yao, L. Sun, C. C. Liu, and F. Zhang, Topological, valleytronic, and optical properties of monolayer PbS, Adv. Mater. **29**, 1604788 (2017).

[73] J. Liu, X. Qian, and L. Fu, Crystal field effect induced topological crystalline insulators in monolayer IV–VI semiconductors, Nano Lett. **15**, 2657 (2015).